Mutations Affecting Symmetrical Migration of Distal Tip Cells in *Caenorhabditis elegans*

Kiyoji Nishiwaki

PRESTO, Japan Science and Technology Corporation and Fundamental Research Laboratories, NEC Corporation, Miyukigaoka, Tsukuba 305, Japan

Manuscript received July 6, 1998
Accepted for publication March 12, 1999

ABSTRACT

The rotational symmetry of the *Caenorhabditis elegans* gonad arms is generated by the symmetrical migration of two distal tip cells (DTCs), located on the anterior and posterior ends of the gonad primordium. Mutations that cause asymmetrical migration of the two DTCs were isolated. All seven mutations were recessive and assigned to six different complementation groups. *vab-3(k121)* and *vab-3(k143)* affected anterior DTC migration more frequently than posterior, although null mutants showed no bias. The other five mutations, *mig-14(k124)*, *mig-17(k113)*, *mig-18(k140)*, *mig-19(k142)*, and *mig-20(k148)*, affected posterior DTC migration more frequently than anterior. These observations imply that the migration of each DTC is regulated differently. *mig-14* and *mig-19* also affected the migration of other cells in the posterior body region. Four distinct types of DTC migration abnormalities were defined on the basis of the mutant phenotypes. *vab-3; mig-14* double mutants exhibited the types of DTC migration defects seen for *vab-3* single mutants. Combination of *mig-17* and *mig-18* or *mig-19*, which are characterized by the same types of posterior DTC migration defects, exhibited strong enhancement of anterior DTC migration defects, suggesting that they affect the same or parallel pathways regulating anterior DTC migration.

Asymmetrical left-right body plan is typical of animal development. However, the plan for anterior-posterior structures is usually asymmetrical. In this regard the *Caenorhabditis elegans* gonad structure is unusual in that the anterior and the posterior U-shaped gonad arms are rotationally symmetrical around the dorsoventral axis at the center of the body (Figure 1). The *C. elegans* gonad is formed so that it folds around the intestine. Relative to the intestine, the anterior arm of the gonad is on the right side of the body cavity and the posterior arm is on the left. The symmetry of the gonad arms is generated by migration of the two mesodermal distal tip cells (DTCs), each located on the anterior or on the posterior ends of the gonad primordium, in a U-shaped pattern during larval development. Therefore, the shape of the gonad arm reflects the migration paths of the DTCs (Kimble and Hirsh 1979; Hedgecock *et al.* 1987). The two DTCs are lineal homologues and originate from the somatic gonad precursor cells Z1 and Z4 by symmetrical divisions during the first larval (L1) stage (Kimble and Hirsh 1979). However, their migration pathways are different from each other: the anterior DTC migrates on the basal lamina of the anterior-right basal surface of the body wall, whereas the posterior DTC migrates on that of the posterior-left.

unc-5, *unc-6*, and *unc-40* are genes required for the circumferential migration of cells and axons in *C. elegans* (Hedgecock *et al.* 1990). UNC-6 is a guidance molecule localized to the basement membrane and homologous to the mammalian netrin (Ishii *et al.* 1992; Serafini *et al.* 1994; Wadsworth *et al.* 1996). UNC-5 and UNC-40 are thought to be UNC-6 receptors expressed on migratory cells (Leung-Hagesteijn *et al.* 1992; Chan *et al.* 1996) and they also have mammalian homologs (Keino-Masu *et al.* 1996; Leonardo *et al.* 1997). Interestingly, although these three genes all affect the migration of both the anterior and posterior DTCs, all the *unc-5*, *unc-6*, and *unc-40* alleles examined affected migration of the posterior DTC more frequently than that of the anterior (Hedgecock *et al.* 1990). These findings suggest that the mechanisms controlling migration of the two DTCs may not always be identical despite the fact that the two cells are homologous to each other in cell lineage and migrate symmetrically during development.

To examine whether molecular mechanisms that control DTC migration are indeed different for each cell, I isolated mutations that cause one cell to migrate differently than the other. Seven mutations in six different genes, including four new genes, were identified in this study. Two of the mutations affected anterior DTC migration more frequently than posterior, and the other five affected the posterior DTC migration more frequently than anterior. This supports the idea that the migration of the two DTCs is regulated differently.

MATERIALS AND METHODS

Strains and culture conditions: The media, culture, and handling of *C. elegans* were described by Brenner (1974).

Address for correspondence: Fundamental Research Laboratories, NEC Corporation, Miyukigaoka, Tsukuba 305, Japan.
E-mail: nishiwak@frl.cl.nec.co.jp

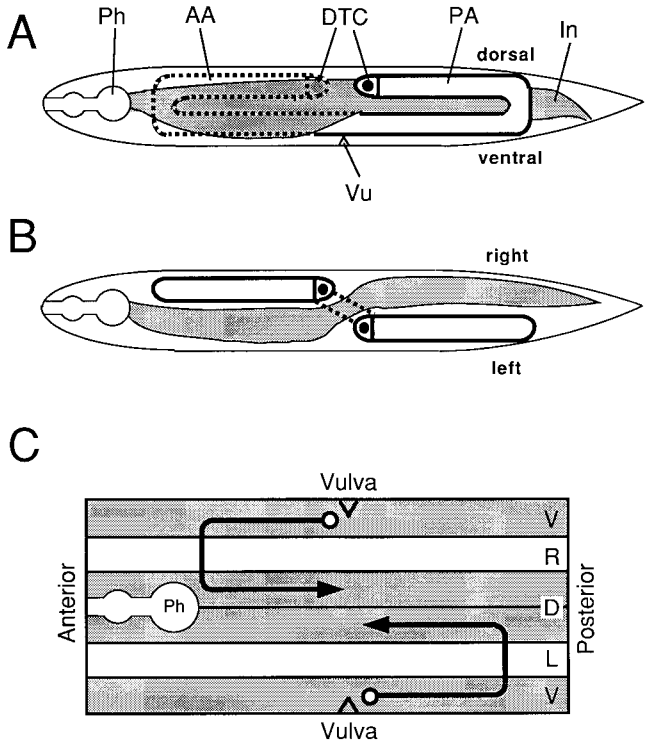

Figure 1.—Schematic presentation of the wild-type hermaphrodite gonad structure. (A) Left lateral view. The intestine is shaded. The posterior arm of the gonad, which is on the left side of the body, is depicted by the solid line, and the anterior arm on the right side by the dotted line. Ph, pharynx; In, intestine; Vu, vulva; DTC, distal tip cell; AA, anterior arm; PA, posterior arm. (B) Dorsal view. (C) Distal tip cell migration in the hermaphrodite shown in cylindrical projection (modified from Hedgecock *et al.* 1987). The projection corresponds to the hermaphrodite body wall cut open at the ventral midline. Dorsal and ventral body wall muscles are shaded. The two DTCs are born around the L1 molt as descendants of two somatic gonad precursor cells, Z1 and Z4, over the ventral muscles (shown by circles) and start to migrate at the mid-L2 stage. They move in opposite directions along the ventral muscles, turn dorsally at the mid-L3 stage, and migrate along the lateral hypodermal cells. They turn again over the dorsal muscles around the L3 molt and migrate toward each other along the dorsal muscles (Hedgecock *et al.* 1987; Antebi *et al.* 1997). Position of vulva in adult is shown. V, ventral; D, dorsal; R, right; L, left.

Mutants were first roughly mapped genetically by the PCR-STS (sequence-tagged site) method using RW7000 as an STS marker strain (Williams *et al.* 1992). They were then mapped more precisely using standard marker mutations and chromosomal deficiencies. The following STSs, mutations, and deficiencies were used:

LGI: *hP4*

LGII: *stP100*, *stP196*, *stP101*, *stP50*, *stP36*, *stP98*, *maP1*, *dpy-10(e128)*, *unc-4(e120)*, *bli-1(e769)*, *rol-1(e91)* (Higgins and Hirsh 1977), *mig-14(mu71)* (Harris *et al.* 1996), *unc-52(e444)*, *mnDf66*, and *mnDf63* (Sigurdson *et al.* 1984)

LGIII: *stP19*, *stP120*, *mgP21*, *stP127*, *stP17*, *tar-1(e1099)* (Hodgkin and Brenner 1977), *dpy-18(e364)*, *unc-71(ay7)* (Chen *et al.* 1997), *unc-25(e156)*, *bli-5(e518)*, *tDf8* (H. Schnabel and R. Schnabel, personal communication), *eDf2* (Hodgkin 1980)

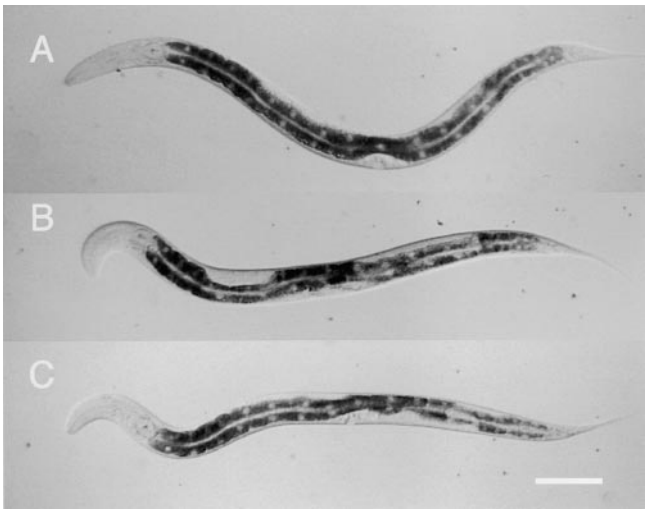

Figure 2.—White patch phenotypes under a dissecting microscope. Anterior to the left, dorsal top. (A) Wild type, (B) an anterior type I defect in *vab-3(k121)*, (C) a posterior type IV defect in *mig-17(k113)*. See Figures 5 and 6 for defective types. Bar, 0.1 mm.

LGIV: *sP4*, *unc-30(e191)*

LGV: *stP192*, *bP1*, *stP6*, *stP108*, *stP105*, *stP128*, *dpy-11(e224)*, *sma-1(e30)*, *him-5(e1490)* (Hodgkin 1980), *unc-76(e911)*, *ctDf1* (Manser and Wood 1990), *arDf1* (Tuck and Greenwald 1995)

LGX: *stP41*, *stP40*, *stP156*, *stP33*, *stP103*, *stP129*, *stP61*, *stP72*, *stP2*, *unc-27(e155)*, *vab-3(e648)* (Lewis and Hodgkin 1977), *egl-15(n484)* (Trent *et al.* 1983), *lin-2(e1309)* (Horvitz and Sulston 1980), *nDf19* (Ambros and Horvitz 1984)

Mutations without a reference are described by Brenner (1974).

Isolation of mutants: Mutations were generated by treating wild-type (N2) hermaphrodites at the fourth larval stage (L4) with ethyl methanesulfonate (EMS) as described by Brenner (1974). Mutants were isolated from animals at the F_2 or F_3 generation. Hedgecock *et al.* (1990) reported that distal tip cell migration defects in *unc-5* or *unc-6* mutant hermaphrodites can be observed by bright-field microscopy at low magnification: the abnormally returned arms of the gonad in *unc-5* and *unc-6* displace the dark intestine dorsally, resulting in the appearance of a white stripe on the ventral side. Therefore, to isolate mutants with abnormal gonad morphology, I looked for animals with dorsal or ventral white patches under a dissecting microscope, especially those with patches either on the anterior or the posterior body region (Figure 2). Animals with a ventral white stripe similar to those seen in *unc-5* or *unc-6* mutants were not picked to avoid isolating alleles of these genes. I screened 230 9-cm plates each of which contained F_2s or F_3s from 200 to 300 F_1s of mutagenized F_0 hermaphrodites. This corresponds to 230 $\times$ 2 $\times$ (200 to 300) = 92,000 to 138,000 genomes. About 4000 candidate animals were isolated and the genetic penetrance of their white patch phenotypes was assessed by examination of the progeny. A total of 103 fertile mutants with misshapen gonad arms were obtained. Of these, 7 were found in which one of the two gonad arms was obviously affected more frequently than the other.

Genetic mapping: Mutants were backcrossed to N2 at least twice to eliminate extraneous mutations. All seven mutations were recessive to their wild-type alleles and affected DTC migration zygotically (data not shown). Genetic mapping was

TABLE 1

Multi-factor PCR STS mapping

	Detection of STS								
Gene			*stP100*	*stP196*	*stP101*	*stP50*	*stP36*	*stP98*	*maP1*	Number[a]
mig-19 II			+	−	−	−	−	−	−	1
			+	+	−	−	−	−	−	3
			+	+	+	−	−	−	−	1
			+	+	+	+	+	−	−	2
			+	+	−	−	−	−	+	1
			+	−	−	−	−	−	+	1
Gene					*stP19*	*stP120*	*mgP21*	*stP127*	*stP17*	Number[a]
mig-18 III					+	+	+	+	−	14
Gene				*stP192*	*bP1*	*stP6*	*stP108*	*stP105*	*stP128*	Number[a]
mig-17 V				+	−	−	−	−	−	7
				+	+	−	−	−	−	1
				−	−	+	+	+	+	3
				−	−	−	+	+	+	10
				−	−	−	−	+	+	7
				−	−	−	−	−	+	8
Gene	*stP41*	*stP40*	*stP156*	*stP33*	*stP103*	*stP129*	*stP61*	*stP72*	*stP2*	Number[a]
vab-3 X	+	−	−	−	−	−	−	−	−	1
	+	+	−	−	−	−	−	−	−	1
	+	+	+	+	−	−	−	−	−	2
	+	+	+	+	+	−	−	−	−	1
	−	−	−	−	−	−	−	−	+	2
Gene	*stP41*	*stP40*	*stP156*	*stP33*	*stP103*	*stP129*	*stP61*	*stP72*	*stP2*	Number[a]
mig-20 X	+	−	−	−	−	−	−	−	−	7
	+	−	−	−	−	−	−	−	+	3
	+	+	−	−	−	−	−	−	+	1
	+	+	+	+	−	−	−	−	−	3
	+	+	+	+	−	−	−	−	+	1
	+	+	+	+	+	−	−	−	−	6
	+	+	+	+	+	−	−	−	+	1
	+	+	+	+	+	+	−	−	−	1
	−	−	−	−	−	−	+	+	+	1
	−	−	−	−	−	−	−	+	+	1
	−	−	−	−	−	−	−	−	+	8

[a] Number of recombinants. Only recombinants were shown.

accomplished using the two-step polymorphic mapping strategy (Williams *et al.* 1992). Mutant alleles were first mapped to a specific chromosome using a single STS particular to each chromosome, *hP4(I)*, *maP1(II)*, *mgP21(III)*, *sP4(IV)*, *bP1(V)*, and *stP103(X)*. This analysis assigned *mig-14(k124)* and *mig-19(k142)* to linkage group II (*LGII*); *mig-17(k113)* to *LGV*; and *vab-3(k121)*, *vab-3(k143)*, and *mig-20(k148)* to *LGX* (data not shown). The data for *mig-18(k140)* were not clear. Assuming that *mig-18* was on the end of a chromosome, the data for *LGII*, *III*, and *X* showed possible linkage. Using multiple STS markers for each of these chromosomes (listed above), *mig-18* was subsequently found to be linked to *stP17* near the right end of *LGIII* (Table 1). Similarly, *mig-19 II*, *mig-17 V*, *vab-3(k121) X*, and *mig-20 X* were further localized on each chromosome using multiple STSs (Table 1). Mutations within the same linkage group, *mig-14* and *mig-19*, as well as *vab-3(k121)* and *mig-20* complemented each other (data not shown).

The data for three-factor mapping experiments with morphological mutations are shown in Table 2. Some two-factor mapping experiments were done for *mig-18*. Of 95 Dpy segregants from + *mig-18/dpy-18* +, 18 were *dpy-18 mig-18/dpy-18* + and 77 were *dpy-18* +/*dpy-18* +. Thus, $2P = 18/95$ and $P = 0.095$. All 205 Mig segregants from + + *mig-18*/+ *bli-5* + segregated only non-Bli progeny. Thus, $2P < 1/205$ and $P < 0.002$.

When nearby deficiencies were available, deficiency mapping was carried out as follows:

mig-19(k142) II: *dpy-10(e128) mig-19*/+ + males were crossed with *mnDf66*/*mnC1 dpy-10(e128) unc-52(e444)* or *mnDf63*/*mnC1 dpy-10(e128) unc-52(e444)* hermaphrodites. *dpy-10* and *mig-19* were about 2 map units apart. The genotype of F_1 *dpy-10 mig-19*/*Df* hermaphrodites was determined by scoring F_2s: the observation that Dpy-10 non-Unc-52 but not

TABLE 2

Three-factor mapping

Genotype of hyterozygote	Phenotype of recombinant	Genotype of recombinant chromosome	Number[a]
+ *mig-17* +/*dpy-11* + *unc-76*	Unc non-Dpy	+ *mig-17 unc-76*	4/12
+ + *mig-14/dpy-10 unc-4* +	Dpy non-Unc	*dpy-10* + *mig-14*	2/2
	Unc non-Dpy	+ *unc-4* +	5/5
+ *mig-14* +/*rol-1* + *unc-52*	Ro1 non-Unc	*rol-1 mig-14* +	16/19
+ + *mig-18/dpy-18 unc-64* +	Unc non-Dpy	+ *unc-64* +	19/19
	Dpy non-Unc	*dpy-18* + *mig-18*	10/10
+ + *mig-18/dpy-18 unc-25* +	Unc non-Dpy	+ *unc-25* +	33/33
	Dpy non-Unc	*dpy-18* + *mig-18*	33/33
+ + *mig-18/unc-71 bli-5* +	Unc non-Bli	*unc-71* + *mig-18*	2/2
+ + *mig-19/dpy-10 unc-4* +	Unc non-Dpy	+ *unc-4* +	12/12
	Dpy non-Unc	*dpy-10* + *mig-19*	13/13
+ *mig-19* +/*unc-4* + *bli-1*	Unc non-Bli	*unc-4 mig-19* +	17/20
+ *mig-20* +/*unc-27* + *lin-2*	Unc non-Lin	*unc-27 mig-20* +	5/18

[a] Number of those with indicated genotype in total number of recombinants isolated.

Dpy-10 Unc-52 animals segregated with the Mig-19 phenotype and dead eggs indicates that the F_1 mother was *dpy-10 mig-19*/*Df*. Of the 46 non-Dpy F_2 segregants from the two F_1 *dpy-10 mig-19*/*mnDf66* animals, 23 showed defects in DTC migration. Many of these DTC migration-defective animals segregated dead eggs, indicating that *mnDf66* deletes *mig-19*. All of the four F_1 *dpy-10 mig-19*/*mnDf63* hermaphrodites and most of their non-Dpy F_2 segregants were normal for DTC migration, but Dpy F_2 segregants often showed the Mig-19 phenotype, indicating that *mnDf63* does not delete *mig-19*.

mig-20(k148) X: Because the males of *mig-20* did not mate, *mig-20* hermaphrodites were crossed with *tra-1(e1099)* males, and F_2 males segregated from F_1 *tra-1*/+; *mig-20*/+ hermaphrodites; that is, pseudo-males homozygous for *tra-1* were crossed with +/*szT1[lon-2(e628)]I; nDf19*/*szT1 X* hermaphrodites. Two F_3 hermaphrodites having DTC migration defects similar to those in *mig-20* were picked. The genotype of these hermaphrodites was *mig-20*/*nDf19*, as shown by the fact that both of them segregated F_4s with the DTC migration defect and dead eggs, but they did not segregate Lon animals. Of the 36 F_4 hermaphrodites that segregated from one animal, 17 exhibited Mig-20 type DTC migration defects. Ten of the 17 animals segregated dead eggs, indicating that *nDf19* deletes *mig-20*.

vab-3(k121 and k143) X: *vab-3(k121)* males were crossed with +/*szT1[lon-2(e628)] I; nDf19*/*szT1 X* hermaphrodites. Three wild-type F_1 hermaphrodites segregated F_2 dead eggs and hermaphrodites with the Vab-3 type DTC migration defect, but did not segregate Lon animals, indicating that these F_1s were *vab-3*/*nDf19*. None of 24 F_2s with the Vab-3 phenotype were found to segregate dead eggs. Thus, *nDf19* appeared to complement *vab-3*. Similarly, *nDf19* was also found to complement *vab-3(k143)*. *nDf19* might be a complex deficiency, because it failed to complement *unc-27* and *mig-20* but not *vab-3*, which is between these two genes.

mig-17(k113) V: *mig-17* males were crossed with *ctDf1 V*/*nT1[unc-?(n754)let-?](IVV)* or *unc-42(e270)arDf1 V*/*nT1[unc-?(n754)let-?](IVV)* hermaphrodites. None of 41 F_1 *mig-17*/*ctDf1* or 36 F_1 *mig-17*/*unc-42 arDf1* animals exhibited the Mig-17 phenotype, indicating that neither *ctDf1* nor *arDf1* deletes *mig-17*.

mig-18(k140) III: *mig-18; unc-4* hermaphrodites were mated with *unc-32(e189)tDf8*/*qC1 dpy-19(e1259)glp-1(q339)* males. None of 32 wild-type F_1 *mig-18(k140)*/*unc-32tDf1; unc-4*/+ hermaphrodites exhibited the Mig-18 phenotype, indicating that *tDf8* does not delete *mig-18*. *mig-18* males were mated with *unc-32(e189) ooc-4(e2078)*/*eDf2 III* hermaphrodites. Ten F_1 hermaphrodites with the Mig-18 phenotype segregated Mig-18 animals and dead eggs, indicating that *eDf2* deletes *mig-18*.

Figure 3 summarizes the positions of the genes on a genetic map determined by the genetic analysis described so far.

Gene dosage experiments: For *mig-18*, *mig-19*, and *mig-20*, the phenotypes over deficiencies were determined. The F_1 segregants from *mig-18*/*eDf2*, *dpy-10 mig-19*/*mnDf66*, or *tra-1*/+; *mig-20*/*nDf19* animals were checked for their gonad phenotypes and cloned in separate plates. F_1s that segregated many F_2 dead eggs were scored as *mig*/*Df* animals.

Analysis of DTC migration phenotypes: Young adult hermaphrodites, which were grown at 16° without starvation, were observed on a 5% agar pad using a Zeiss Axiophoto microscope equipped with a Plan 100 objective and Nomarski differential interference contrast optics (Sulston and Horvitz 1977). The trajectories of the DTCs were deduced from the shapes of the gonad arms. I sometimes observed mutant animals with anterior arms on the left side or those with posterior arms on the right side. These phenotypes might be caused by the mispositioning of the gonad primordium at the L1 stage (E. M. Hedgecock, personal communication). The migration of DTCs on arms formed on the wrong side and that of their counterparts on the normal-sided arms were similarly affected by the mutations. This type of abnormality was not seen in more than 200 wild-type animals scored. The frequencies of misplaced arms in 200 animals examined for each mutant were as follows (where R stands for cases where the posterior arm was on the right side and L where the anterior arm was on the left side): *vab-3(e648)*, 4%(R) and 1%(L); *vab-3(k143)*, 2%(R); *mig-20*, 3%(R); *mig-14(k124)*, 3%(R) and 2%(L); *mig-14(mu71)*, 1%(R) and 2%(L); *mig-19*, 3%(R); *vab-3(e648); mig-14(k124)*, 2%(R) and 5%(L); *vab-3(e648); mig-17*, 6%(R) and 2%(L); *vab-3(e648); mig-18*, 8%(R) and 1%(L); *vab-3(e648); mig-19*, 11%(R) and 1%(L); *vab-3(e648); mig-20*, 2%(R); *mig-14(k124); mig-17*, 3%(R) and 2%(L); *mig-14(k124); mig-18*, 1%(R) and 2%(L); *mig-14(k124); mig-20*, 2%(R) and 3%(L); *mig-20; mig-17*, 1%(R); *mig-20; mig-19*, 6%(R) and 1%(L). Strains with *vab-3(k121)*; *mig-17; mig-18* and *mig-17; mig-19* were not scored.

To determine the antero-posterior position of the first turn

of the DTCs, L3 larvae whose posterior gonad arms had just turned were examined. Position was assessed relative to that of the postdeirid neurons (Sulston and Horvitz 1977).

Scoring of non-DTC cell migration: Late L1 animals grown at 16° were examined by Nomarski microscopy. Migration of HSN, ALM, CAN, QR/L, and embryonic coelomocyte mother cells was scored by their final positions or positions of their descendants relative to those of the stationary Vn.a and Vn.p hypodermal cells as described by Harris *et al.* (1996). Male linker cell migration was assessed by gonad morphology in a *him-5(e1490)* background for all mutations except for *mig-17(k113)*.

Construction of double mutants: To combine mutations of different linkage groups, other than *vab-3(e648)*, recessive marker mutations were used which were both *trans* to and closely linked to each of the two mutations. Double mutants were isolated as clones that did not segregate marker mutations from the progeny of the double *trans*-heterozygotes listed below. The *mig-18; mig-19* double was not able to be established as a line because it was sterile. Double mutants segregated with a reasonable frequency from the double *trans*-heterozygotes, that is, about 1/16 of the segregants. For each combination, at least two independently isolated double mutants were checked for their DTC phenotypes. Double mutants carrying *vab-3(e648)* and other unlinked mutations were generated using the abnormal head morphology of *vab-3* and various mutant phenotypes described in Results.

Double *trans*-heterozygotes are as follows:

vab-3(k121)/egl-15; mig-14(k124)/unc-52
vab-3(k121)/egl-15; mig-17(k113)/sma-1
vab-3(k121)/egl-15; mig-18(k140)/unc-25
vab-3(k121)/unc-27; mig-19(k142)/unc-4
mig-14(k124)/unc-52; mig-17(k113)/sma-1
mig-14(k124)/unc-52; mig-18(k140)/unc-25
mig-14(k124)/unc-52; mig-20(k148)/unc-27
mig-17(k113)/sma-1; mig-18(k140)/unc-25
mig-17(k113)/sma-1; mig-19(k142)/unc-4
mig-17(k113)/sma-1; mig-20(k148)/unc-27
mig-18(k140)/unc-25; mig-19(k142)/unc-4
mig-18(k140)/unc-25; mig-20(k148)/unc-27
mig-19(k142)/unc-4; mig-20(k148)/unc-27

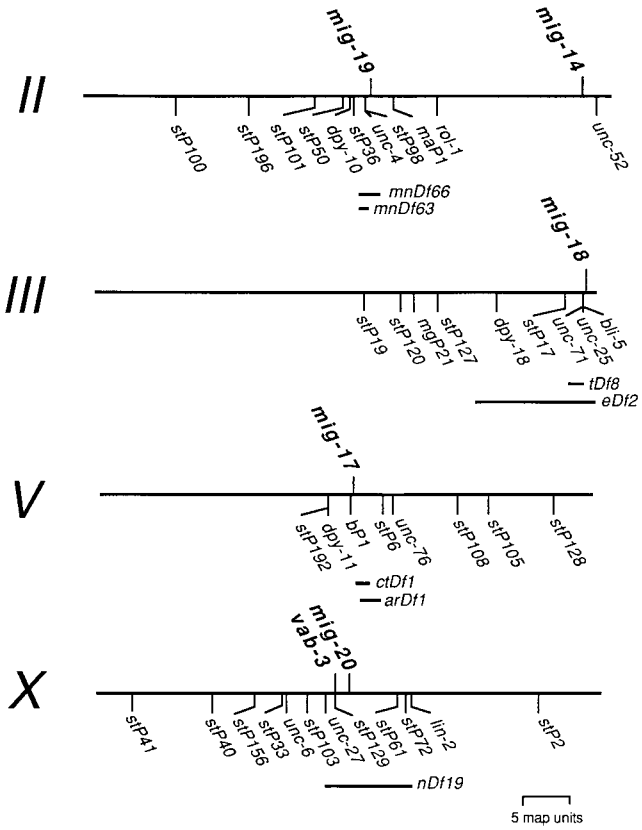

Figure 3.—Genetic mapping. *mnDf66* deletes *mig-19*, but *mnDf63* does not. *eDf2* deletes *mig-18*, but *tDf8* does not. Neither *ctDf1* nor *arDf1* deletes *mig-17*. *nDf19* deletes *mig-20*, but not *vab-3* (anomalous). Map position for *vab-3* is from ACeDB data base.

Construction of double mutants of the same linkage group was carried out as follows. To generate double mutants of *mig-20(k148)* and *vab-3(k121)* or *vab-3(e648), unc-27 mig-20(k148)* hermaphrodites were crossed with *vab-3(k121)* or *vab-3(e648)/+; tra-1(e1099)* males and wild-type F_1 *unc-27 + mig-20(k148)/+ vab-3 +* hermaphrodites were obtained. F_2 non-Unc hermaphrodites with the Mig-20 phenotype (posterior type III defect not seen in *vab-3*), which were expected to be *+ vab-3 mig-20/unc-27 + mig-20* or *+ + mig-20/unc-27 + mig-20*, were isolated. F_3 hermaphrodites that segregated only non-Unc progeny exhibiting DTC migration defects characteristic both for *vab-3(k121)* and *mig-20* or head abnormality characteristic for *vab-3(e648)* were selected.

To generate *mig-19(k142)* and *mig-14(k124)* doubles, *rol-1 mig-14* hermaphrodites were crossed with *mig-19/+* males (*k142* homozygous males are sterile) and wild-type F_1 *+ rol-1 mig-14/mig-19 + +* hermaphrodites were selected on the basis of segregation of the Mig-19 phenotype. Six F_2 non-Rol hermaphrodites with the Mig-14 phenotype (posterior type II defect not seen in *mig-19*), which were expected to be *mig-19 + mig-14/+ rol-1 mig-14*, were isolated. *mig-19 mig-14* doubles were isolated as F_3 hermaphrodites that only segregated non-Rol progeny.

Double mutants carrying *mig-14*, *-19*, or *-20* were further confirmed by phenotypes in addition to DTC migration, as described in results.

RESULTS

Mutations affecting symmetrical migration of DTCs: I isolated mutations that differentially affected the morphologies of the anterior and the posterior gonad arms. Mutants were initially selected by their white patch phenotypes, which are often due to defects in the morphogenesis of the gonad arms (see materials and methods). Subsequently, the gonad morphogenesis of these mutants was analyzed by Nomarski microscopy. I identified seven mutations that asymmetrically affected the shapes of the two gonad arms. All of these mutations were recessive and fell into six different complementation groups. The mutations were designated *k113*, *k121*, *k124*, *k140*, *k142*, *k143*, and *k148*. *k121* was mapped to the right arm of *LGX*, which contains *vab-3*, a mutation that results in a similar phenotype (A. Chisholm, personal communication). Both *k121* and *k143* failed to complement the *e648* allele of *vab-3*, a gene previously identified by mutations affecting head morphogenesis (Lewis and Hodgkin 1977) and which has been reported to have a DTC migration defect as well (Hedgecock *et al.* 1987; Chisholm and Horvitz 1995; Zhang and Emmons 1995). *k124* was found to be an allele of *mig-14*, a gene originally identified by a muta-

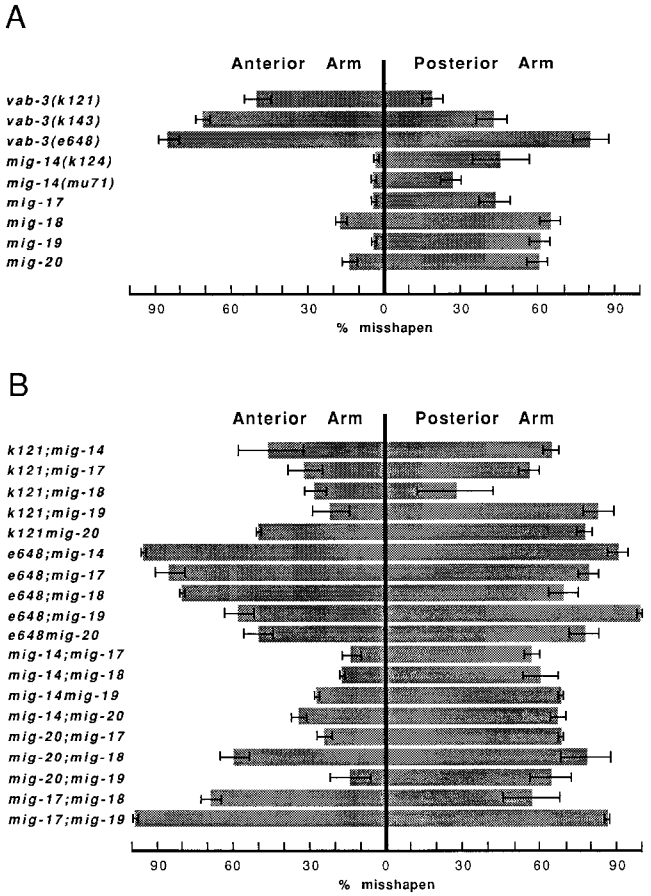

Figure 4.—Effects of mutations on anterior and posterior DTC migration. (A) Asymmetrical effects of single mutations on DTC migration. (B) Effects of double mutant combinations on DTC migration. *k121* and *e648* are *vab-3* alleles. The *mig-14* allele is *k124*. Two independent sets of 100 animals were scored for each mutant. Average percentage of animals with misshapen anterior or posterior gonad arms in each of the mutants is indicated by the shaded bar and the SD by the thin line. No abnormalities were observed in more than 200 wild-type animals examined.

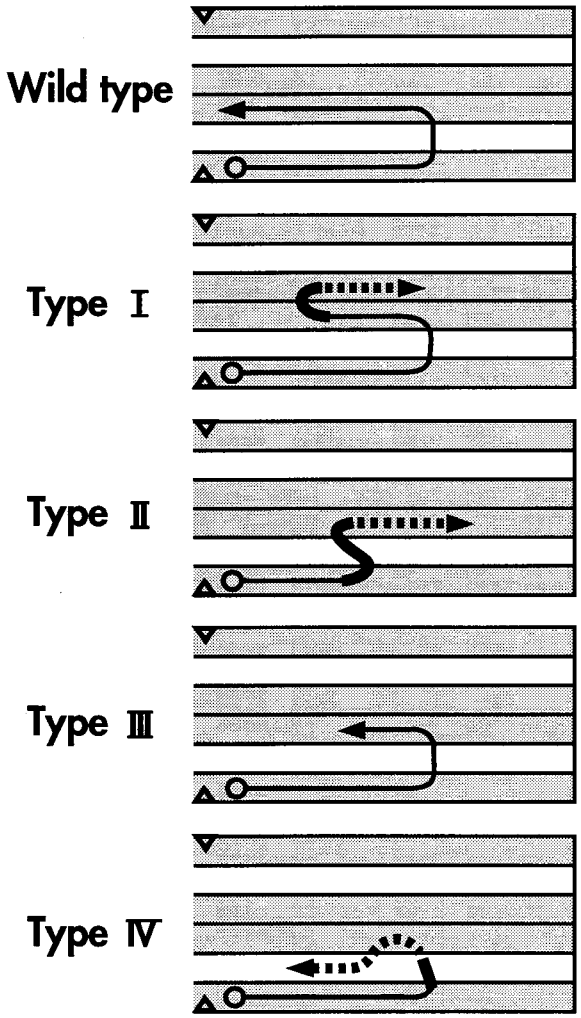

Figure 5.—Four types of DTC migration abnormalities. Defective patterns are shown for the posterior gonad arm, although the defects could be in the anterior or posterior arm depending on the mutations and individuals. The normal part of the migration path is shown by a thin line and the abnormal part by a bold line. The dotted line indicates that this section of the migration path could be variable.

tion that results in migration defects in several neurons and neuroblasts (Harris *et al.* 1996). The other four mutations, *k113*, *k140*, *k142*, and *k148* seemed to define four new genes *mig-17*, *mig-18*, *mig-19*, and *mig-20*, respectively, judging from their associated phenotypes and genetic map positions (Figure 3).

Characterization of mutant DTC migration phenotypes: DTC migration abnormalities were determined from the shape of the mutant gonad arms. As shown in Figure 4A, of the seven mutations isolated only *vab-3* alleles *k121* and *k143* affected the anterior DTC more frequently than the posterior, although *vab-3(e648)* affected both similarly. Mutations in the other five genes affected the posterior DTC more frequently than the anterior. *mig-14(mu71)* (Harris *et al.* 1996) was found to affect the posterior DTC more frequently. The asymmetric influence was especially noticeable in the *mig-14*, *mig-17*, and *mig-19* animals. None of the mutations were fully penetrant. I categorized the mutant DTC migration abnormalities into four distinct types, from I to IV, as shown in Figure 5. In the type I defect, DTCs initially turned twice, as seen in normal animals, but after the second, they often turned around on the dorsal muscles and migrated in the opposite direction. In the type II defect, DTCs turned with an acute angle at the first turn. The second turn on the dorsal muscles was similarly acute, but followed by a turn in the opposite direction. In the type III defect, the DTCs prematurely ceased their migration on the dorsal muscles after the second turn. The distal arm of the gonad usually swelled afterward, probably because of the proliferation of germ cells. In the type IV defect, DTCs appeared to deviate from their correct migration path after the first turn. They initially moved dorso-anteriorly after the first turn and then migrated anteriorly while meandering over

TABLE 3

Classification of genes by the types of mutant DTC migration abnormalities

		Frequency for each defective type[a]										
		Anterior DTC					Posterior DTC					Anterior shift of first turn[b]
Gene	Allele	I	II	III	IV	M	I	II	III	IV	M	
vab-3	*k121*	36	0	0	0	10	10	0	0	0	6	0 (n = 50)
	k143	65	0	0	0	4	33	1	0	2	2	ND
	e648	52	5	0	3	22	53	9	0	3	11	11 (n = 57)
mig-20	*k148*	10	0	1	0	2	42	0	12	0	3	8 (n = 60)
mig-14	*k124*	0	1	0	0	1	8	41	0	0	5	49 (n = 72)
	mu71	1	1	0	0	2	9	13	0	0	6	ND
mig-17	*k113*	0	0	0	1	3	7	0	1	32	7	4 (n = 55)
mig-18	*k140*	2	0	0	0	13	3	0	4	37	18	4 (n = 54)
mig-19	*k142*	0	0	1	2	0	4	0	3	32	24	21 (n = 73)

The score for wild type was 0% (n = 68). n, number of animals examined; ND, not determined.

[a] Percentage of the anterior or the posterior DTCs that showed the types of migration abnormalities listed in Figure 5 (from I to IV). M, miscellaneous defects that were not categorized. Data are underlined when more than 20%. One hundred animals were examined for each mutant.

[b] Percentage of the posterior DTCs turned at or anterior to the postdeirid neurons.

the dorsal muscles or the lateral hypodermal cells, but not along the dorsal muscles as in the wild type.

Although every mutant exhibited multiple types of DTC migration abnormalities, one or two major types of abnormalities were prevalent for different mutants. On the basis of the most frequently observed abnormal patterns of DTC migration, the mutations were classified into four classes (Table 3). *vab-3(k121)*, *vab-3(k143)*, and *vab-3(e648)* caused a major anterior type I defect (plus a major posterior type I defect in the cases of *k143* and *e648*) and they constituted the first class. *mig-20(k148)* resulted in a major posterior type I defect and it constituted the second class. *mig-14(k124)* and *mig-14(mu71)* caused a major posterior type II defect and constituted the third class. *mig-17(k113)*, *mig-18(k140)*, and *mig-19(k142)* all resulted in a major posterior type IV defect and they constituted the fourth class. None of the newly isolated mutants exhibited any gross abnormality in body morphology. Phenotypes other than the cell migration abnormalities are listed in Table 4.

vab-3(k121, k143): Anterior and posterior type I DTC migration defects were often seen in these mutants (Figure 6B). *vab-3* encodes a transcription factor of the Pax6 family found in mammals and Drosophila (Chisholm and Horvitz 1995). *e648* is a nonsense mutation that deletes part of the paired domain and the whole homeodomain of the polypeptide (Chisholm and Horvitz 1995), suggesting that it is a null allele. In contrast to *e648*, *k121* did not have any abnormalities in head morphology and *k143* had weak abnormalities in it. While the extra turns in DTC migration usually occurred only once in *k121* or *k143*, one or two additional turns were often observed in *e648*. Although *k121* and *k143* asymmetrically affected the anterior and posterior DTCs (*k121*, 50 ± 5% for anterior and 19 ± 4% for posterior; *k143*, 71 ± 2% for anterior and 42 ± 6% for posterior), *e648* similarly affected both and the effect was more penetrant (85 ± 4% for anterior and 81 ± 7% for posterior; Figure 4A). The score for the heterozygote *k121/e648; unc-30/+* was 46% (n = 50) for anterior

TABLE 4

Other defects

Mutants	Locomotion	Egg laying	Other
vab-3(k121)	+	+	Not detected
vab-3(k143)	+	+	Head and copulatory spicule morphology weakly defective
mig-14(k124)	Weak Unc	+	Vulval morphology weakly defective
mig-17(k113)	+	+	Not detected
mig-18(k140)	+	+	Not detected
mig-19(k142)	Weak Unc	Weak Egl	Copulatory spicule morphology defective
mig-20(k148)	Weak Unc	Weak Egl	Copulatory spicule and fan morphology defective

Unc, uncoordinated movement; Egl, egg-laying defective.

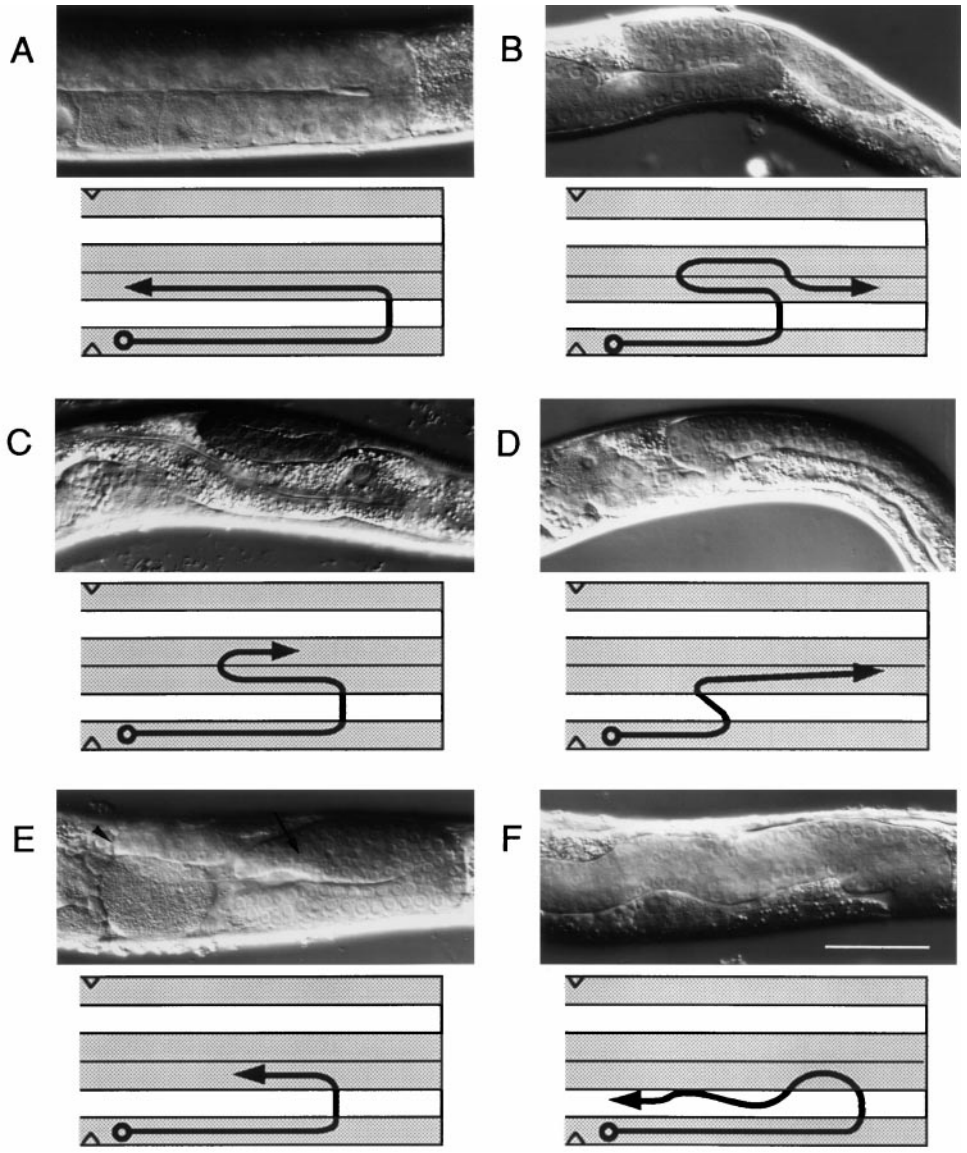

Figure 6.—DTC migration-defective phenotypes. The photos are of wild-type and mutant animals with representative phenotypes and show the posterior left side of the animals except for C, which is posterior right. (A) Wild type. (B) Type I defect in *mig-20(k148)*. Similar phenotypes were frequently observed in the anterior or posterior arms of *vab-3* mutants. (C) Type I defect in *mig-20(k148)*. (D) Type II defect in *mig-14(k124)*. (E) Type III defect in *mig-20(k148)*. This animal has branched distal arms; the arrowhead indicates the DTC on one branch, and the arrow indicates the other branch without a DTC. (F) Type IV defect in *mig-18(k140)*. Similar phenotypes were often displayed by *mig-17(k113)* and *mig-19(k142)*. Bar, 50 μm.

and 36% (n = 50) for posterior, and that for *k143*/*e648; unc-30*/+ was 87% (n = 82) for anterior and 67% (n = 82) for posterior. Therefore, *k121* and *k143* seemed to be weaker than *e648*.

mig-20(k148): The posterior type I defect was most prominent. Anterior type I and posterior type III defects were also observed (Figure 6, B, C, and E). Although both *mig-20* and *vab-3* exhibited the type I defect, their phenotypes were not always the same; in *mig-20* DTC migration often ceased shortly after the turn on the dorsal muscles (Figure 6C), whereas in *vab-3(k121)* or *vab-3(k143)* migrations continued to move toward the head or the tail (Figure 6B). In addition to these DTC migration abnormalities, the posterior gonad arms of *k148* often bifurcated after the second turn. In such cases, a DTC was found on the tip of one of the two branches while the other branch had no DTC (Figure 6E). I deduced the trajectory of the DTC from the shape of the branch bearing the DTC. The DTC-less branch extended toward the anterior to various extents. The mechanism of migration in the DTC-less branch is not known. In *k148*/*nDf19*, 19% (n = 91) exhibited defects in the anterior arm and 44% (n = 91) exhibited defects in the posterior arm. The posterior arm defect in *k148*/*nDf19* seems to be weaker than that of *k148* homozygote (14 ± 3% for the anterior arm and 60 ± 4% for the posterior), suggesting that *k148* may not be a simple loss-of-function mutation.

mig-14(k124): Although *k124* appeared to be stronger than *mu71*, both of these alleles showed similar phenotypic characteristics. The posterior type II defect was the most prominent (Figure 6D) and the posterior type I defect was also observed. The migration distances of DTCs on the ventral muscles were frequently shorter than in wild type (Table 3). Although no deficiency that deletes the *mig-14* locus is available, independent isolation of two different alleles, both of which have similar phenotypic characteristics, supports the idea that *k124* is a loss-of-function mutation.

mig-17(k113), mig-18(k140), and mig-19(k142): The pos-

A

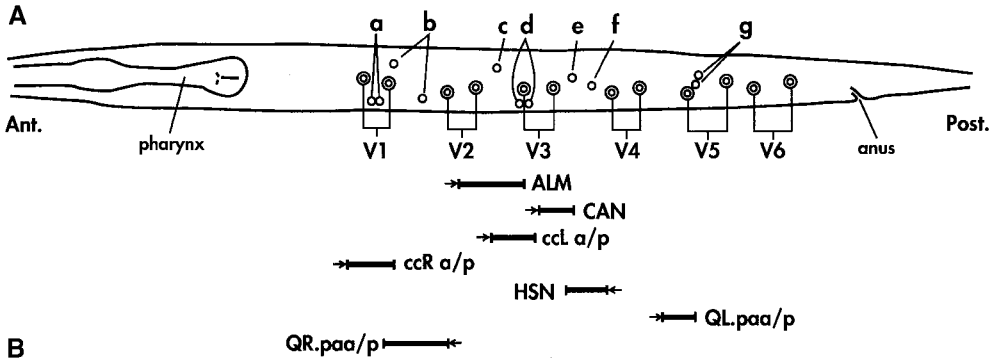

B

Cells \ Mutants	*vab-3(k121)*	*mig-14(k124)*	*mig-17(k113)*	*mig-18(k140)*	*mig-19(k142)*	*mig-20(k148)*
ALM	0 (44)	4 (47)	0 (51)	2 (49)	0 (50)	9 (56)
CAN	0 (44)	2 (47)	0 (51)	0 (49)	0 (50)	5 (45)
ccL a/p	5 (20)	0 (26)	11 (27)	4 (26)	13 (23)	71 (31)
ccR a/p	0 (24)	0 (40)	0 (24)	0 (23)	0 (27)	4 (25)
HSN*	5 (44)	91 (47)	8 (51)	6 (49)	58 (50)	39 (56)
QL.paa/p*	0 (20)	100 (26)	0 (27)	0 (26)	0 (23)	0 (31)
QR.paa/p*	0 (24)	100 (40)	0 (24)	17 (23)	0 (27)	64 (25)
linker cell	0 (30)	42 (48)	0 (30)	13 (30)	12 (57)	0 (38)

Figure 7.—Other cell migration defects in mutants. (A) Schematic presentation of lateral view of wild-type late L1 hermaphrodite. Vn.a/p hypodermal cells used for local markers of A/P axis are shown. Positions of left and right lateral neurons and coelomocytes, which were scored in this experiment, in a representative wild-type animal are depicted together, although they are not always in the same focal plane (modified from Sulston and Horvitz 1977). (a) ccRa/p, (b) QR.paa/p, (c) ALM, (d) ccLa/p, (e) CAN, (f) HSN, and (g) QLpaa/p. Cell names with L or R except for ALM mean the cells are at the left or right side of the body and those without these letters and ALM are bilaterally symmetrical. Positional ranges of these cells in 40 wild-type animals examined are shown by bold lines beneath the drawing. An arrow next to the range stands for direction of migration of the cell(s) and/or its precursor cell. (B) Percentage of animals with cells out of the wild-type range is shown next to the number of animals examined (in parentheses). Migration of linker cells is not shown in A and was scored by examining the shape of the adult male gonads. Asterisks indicate cells and/or precursors of the cells that migrate from the posterior body region.

terior type IV defect was most frequent (Figure 6F) and the posterior type I defect was also observed. *mig-18* and *mig-19* also had various defects in the anterior as well as the posterior DTC migrations. Of the *mig-18(k140)/eDf2* animals, 16% (n = 111) had defects in the anterior and 70% (n = 111) had defects in the posterior arms. The score does not seem to be significantly different from that of the *k140* homozygote (17 ± 2% for anterior and 65 ± 4% for posterior), consistent with *k140* being a complete loss-of-function (null) or a near null allele. In *mig-19*, the location of the first turn of the DTCs on the ventral muscles was often anterior to the wild-type position (Table 3). Of the *k142/mnDf66* animals, 18% (n = 134) exhibited defects in the anterior arm and 45% (n = 134) in the posterior arm. Because this phenotype is weaker than that exhibited by the *k142* homozygote for the posterior arm (4 ± 1% for anterior and 61 ± 4% for posterior), *k142* does not appear to be a simple loss-of-function allele.

Migration abnormalities in other cell types: To ask whether these mutations affecting DTC migration affected the migration of other cell types as well, I examined eight different cells that migrate during embryonic and postembryonic development (Figure 7).

Penetrant cell migration defects were found in *mig-14*, *mig-19*, and *mig-20*. In *mig-14(k124)*, most of the animals exhibited HSN and QL.pa and QR.pa descendants migration defects. HSN was often too posterior. In all the animals examined, the positions of QR.pa descendants were posterior to wild type and were around the hypodermal cell V3. QL.pa descendants were also found around V3, suggesting that the direction in which QL and/or its descendants migrate was reversed, because QL is the sister of V5 and is produced just anterior to it and, in the wild-type case, subsequently migrates in a posterior direction (Sulston and Horvitz 1977). Migration of the male linker cell was also affected in *mig-14*. In *mig-19(k142)*, the position of HSN was often too posterior. In *mig-20(k148)*, HSN migration was also affected, with the QR.pa descendants frequently found located between V2 and V3. In addition to these defects, ccLa/p cells in *mig-20* were frequently found in a position more anterior than their wild-type counterparts.

The effect of double mutants on asymmetrical DTC migration: Double mutants were generated using six of the seven mutations isolated in this study and *vab-3(e648)*. Stable double mutants were successfully constructed for all the combinations except *mig-18(k140); mig-19(k142)*, which was sterile. The frequencies of misshapen arms observed in these double mutants are summarized in Figure 4B. When *vab-3(k121)* was combined with each of the other five mutations, the asymmetrical migration phenotypes became less pronounced. When two of the latter five mutations were combined, the effects on anterior DTC migration were often enhanced. The enhancement of the anterior DTC migration defect was especially evident in *mig-20; mig-18*, *mig-17; mig-18*, and *mig-17; mig-19* double mutants.

TABLE 5

DTC migration abnormalities in double mutants

Genotype	Frequency for each defective type[a]										Anterior shift of first turn[b]
	Anterior DTC					Posterior DTC					
	I	II	III	IV	M	I	II	III	IV	M	
vab-3(k121)	36	0	0	0	10	10	0	0	0	6	0 (n = 50)
vab-3(k121); mig-14	38	0	0	0	8	49	9	2	1	1	21 (n = 58)
vab-3(k121); mig-17	5	0	0	15	12	0	0	1	45	9	ND
vab-3(k121); mig-18	2	0	0	8	16	3	0	0	5	17	ND
vab-3(k121); mig-19	9	0	4	2	7	14	0	8	38	21	ND
vab-3(k121) mig-20	25	0	17	0	7	57	0	14	1	3	ND
vab-3(e648)	52	5	0	3	22	53	9	0	3	11	11 (n = 57)
var-3(e648); mig-14	75	2	0	0	18	57	7	1	2	20	16 (n = 57)
vab-3(e648); mig-17	33	11	2	15	19	30	7	4	25	12	ND
vab-3(e648); mig-18	23	3	5	23	28	24	5	6	28	9	ND
vab-3(e648); mig-19	20	1	9	2	22	33	46	4	2	14	10 (n = 71)
vab-3(e648) mig-20	49	0	1	0	10	60	3	1	1	13	ND
mig-14	0	1	0	0	1	8	41	0	0	5	49 (n = 72)
mig-14; mig-17	4	1	1	3	3	8	22	0	7	11	51 (n = 61)
mig-14; mig-18	1	1	0	6	9	5	33	1	1	16	35 (n = 62)
mig-14 mig-19	0	0	3	13	8	1	53	6	6	1	74 (n = 57)
mig-14; mig-20	5	1	6	8	11	4	24	4	12	19	66 (n = 62)
mig-20	10	0	1	0	2	42	0	12	0	3	8 (n = 60)
mig-20; mig-17	7	0	3	9	5	12	0	11	30	16	ND
mig-20; mig-18	7	6	3	16	28	15	5	8	18	20	ND
mig-20; mig-19	0	0	4	3	7	17	0	19	11	16	ND
mig-17	0	0	0	1	3	7	0	1	32	7	4 (n = 55)
mig-17; mig-18	2	0	0	52	13	7	1	1	35	14	ND
mig-17; mig-19	0	0	2	92	6	6	0	4	61	19	ND

[a] Same as in Table 3. To make it easier to compare with single mutant phenotypes, some single mutant data in Table 3 are also shown here.

[b] Same as in Table 3. The *mig-14* allele is *k124*. Intermediate phenotypes between I and II were included in M. This was most frequently observed in posterior DTC in *mig-14; mig-18* and was 7%.

Phenotypic suppression was observed between the mutant classes: A detailed analysis of the DTC migration phenotypes of double mutants is shown in Table 5. The double mutants generally exhibited more divergent phenotypes than each single mutant and were not simply additive (compare Tables 3 and 5). However, focusing on the major phenotypes, which were observed in >20% of individuals, I observed phenotypic suppression between some of the mutant classes as follows: (1) Both *vab-3(k121)* and *vab-3(e648)* alleles suppressed the posterior type II defect of *mig-14*. The first dorsalward turn of the posterior DTC was anterior to the postdeirid neurons in 21% of the *vab-3(k121); mig-14* animals and in 16% of the *vab-3(e648); mig-14* animals (Table 5). Thus, *vab-3* also seemed to partly suppress this *mig-14* phenotype (Table 3). (2) *mig-17*, *-18*, and *-19* suppressed the anterior type I defect associated with the weak *vab-3(k121)* allele, but its effect on the anterior and posterior type I defects of the strong *vab-3(e648)* allele was not clear. (3) The posterior type IV defect of *mig-19* was suppressed, and the weak posterior type II defect of *vab-3(e648)* was enhanced in *vab-3(e648); mig-19* mutants. *vab-3(e648)* seems to partly suppress the anterior shift of the dorsalward turning point of the posterior DTC in *mig-19* (compare Tables 3 and 5). (4) *mig-14* suppressed the posterior type IV defect of *mig-17*, *-18*, and *-19*. (5) *mig-14* suppressed the posterior type I defect of *mig-20*.

Strong enhancement of type IV defect observed in double mutants consisting of *mig-17* and *mig-18* or *mig-19*: *mig-17*, *-18*, and *-19* are mutations within the same class characterized by a posterior type IV defect. In *mig-17; mig-18* and *mig-17; mig-19* double mutants, this type IV defect was strongly enhanced, especially in the anterior arm. This effect was very evident for the *mig-17; mig-19* double mutants, where 92% of anterior arms showed the type IV defect. I did not score the phenotype for the *mig-18; mig-19* doubles, because the animals were sick and sterile, and often were found to be ruptured at the vulva, suggesting that their gonads were severely affected or that vulval development was abnormal.

Double mutants consisting of *mig-20* and *mig-14* or

***mig-19* exhibit strong uncoordinated movement phenotype:** *mig-20* and *mig-14* mutations exhibited slightly uncoordinated movement. However, when combined, the double *mig-20; mig-14* and *mig-20; mig-19* mutants displayed a strong uncoordinated movement phenotype. The *mig-20; mig-19* double mutant was small, sluggish, moved very little, rarely moved backward, and often shrank. The *mig-20; mig-14* mutant moved slightly better than did *mig-20; mig-19* and had a normal body size. *mig-14; mig-19* double mutants were not more uncoordinated than *mig-14* single mutants.

DISCUSSION

Seven mutations in six genes asymmetrically affecting the migration of the two DTCs during development were isolated in this study. Two mutations in *vab-3* affected migration of the anterior DTC more often than the posterior, and the other five affected the posterior DTC more often than the anterior. These results suggest that the migration of the two DTCs is regulated differently and that the symmetrical development of the gonad arms is governed by an elaborate genetic system. It is possible that there are more genes whose mutations more strongly alter posterior DTC migration than genes that have the opposite effect. In monodelphic nematodes, which develop a single-armed gonad, the single arm is always anterior, and the posterior DTC generated from Z4 often undergoes programmed cell death (Sternberg and Horvitz 1981; Felix and Sternberg 1996). Although *C. elegans* is didelphic, its posterior arm might have an evolutionarily conserved bias to degenerate.

The weak *vab-3* alleles *k121* and *k143* affected the anterior DTC more frequently than the posterior, while the strong *vab-3(e648)* affected both similarly. Another strong allele *k109* isolated in the present screening also produced a highly penetrant effect on both DTCs (K. Nishiwaki, unpublished results). Therefore, it is possible that the asymmetrical effect of *vab-3* may be visible only for weak alleles. *vab-3*, which encodes a Pax6 family protein, has been reported to be expressed mainly in many neurons and most of the hypodermal cells in the anterior half of the body (Chisholm and Horvitz 1995). The stronger effect of *k121* and *k143* on the anterior DTC might reflect the asymmetrical distribution of the VAB-3 protein.

DTC migration defects were classified into four distinct types. The type I defect was often observed in *vab-3(k121)* and *mig-20(k148)*. One characteristic feature is a radical extra turn on the dorsal muscles that is so radical that it suggests a certain repulsive activity may be generated at the region where the turn occurs. The wild-type *vab-3* and *mig-20* gene products may function to suppress the generation of this repulsive activity and to make DTCs move straight along the dorsal muscles. Two mutations that affect sex myoblast migration, *egl-15* and *egl-17*, are known to change an attractive interaction to a repulsive one (Stern and Horvitz 1991).

The type II defect was mostly specific to strains of a *mig-14* background and in *vab-3(e648); mig-19* double mutants, and this defect was observed in the posterior DTC. *mig-14(k124)* also had QL/R neuroblast migration defects. The same Q cell migration abnormalities have been reported in *mig-14(mu71)* animals (Harris *et al.* 1996). *mig-14* is proposed to be involved in the *mab-5* pathway because the *mig-14(mu71)* mutation represses *mab-5* expression in QL, thereby affecting QL migration (Harris *et al.* 1996). *mig-14* also acts in a *mab-5*-independent manner to determine the final positions of QR descendants in the antero-posterior axis: the final positions of QR descendants are shifted posteriorly in *mig-14* mutants whether or not *mab-5* activity is present (Harris *et al.* 1996). Because the *mab-5* null mutant *e1239* is normal for DTC migration (Kenyon 1986; K. Nishiwaki, unpublished results) and *mab-5* does not seem to be expressed in DTCs (Cowing and Kenyon 1992; Salser *et al.* 1993; Salser and Kenyon 1996), the function of *mig-14* in DTC migration is likely to be independent of *mab-5*. Although it is not clear whether the positioning function of *mig-14* proposed for Q cells also operates in DTCs, the shortened migration distance of the posterior DTC on the ventral muscles in *mig-14*, which is due to an anterior shift of the dorsalward turning point, suggests this possibility. It remains to be determined whether the posterior DTC migrates more slowly in *mig-14* than in wild type or if migration ceases precociously, so that the migration distance becomes shortened. Although *vab-3(e648); mig-19* also showed a type II defect, it was not always associated with a shortening of the migration distance on the ventral muscles. This was also the case for *vab-3; mig-14* double mutants, 20% of which exhibited shortened migration, but fewer than 10% of which had type II defects. These results suggest that the two phenotypes, the type II defect and the shortened migration on the ventral muscles, may be separable.

The type III defect was most frequently exhibited by *mig-20* and double mutants carrying *mig-20*. The type was characterized by premature halt in migration, and this phenotype was also observed in HSN, QR.pa, and ccLa/p mother cell migrations; *mig-20* function may be needed for cells to migrate normal distances.

The type IV defect was often seen in *mig-17*, *-18*, and *-19* mutants. It appears that the guidance cues on basal laminae of the lateral hypodermal cells and the dorsal muscles for DTC migration, or recognition of these guidance cues by the DTC, had became obscured in these mutants. I found that a combination of *mig-17* and *mig-18* or *mig-19* strongly enhanced the type IV defect. Surprisingly, this enhancement was especially prominent in the anterior DTC, in spite of the fact that the defect could seldom be observed in any of the three single mutants. This suggests that these three mutations

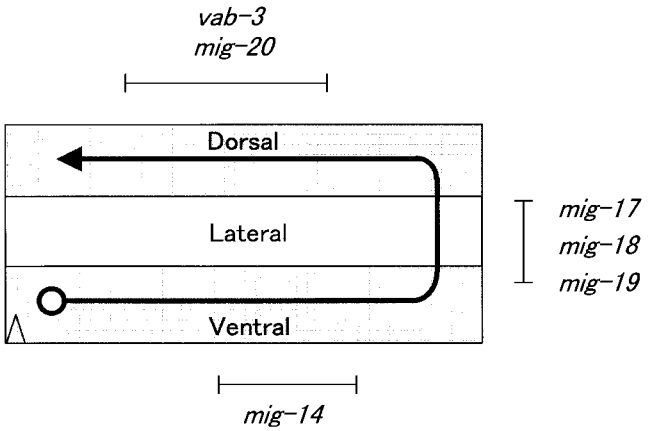

Figure 8.—Chronology of onset of major defective events. Approximate duration when defects are first visible for each mutation is plotted on the wild-type DTC path.

affect the same or parallel pathways regulating anterior DTC migration.

Phenotypic suppression was found between some of the mutant classes. *mig-14* suppressed *mig-17*, *mig-18*, *mig-19*, and *mig-20*. This might reflect the chronological order in which each of the major defective events in DTC migration caused by the respective mutations occurs (Figure 8). That is, *mig-14* affects DTC migration prior to the first DTC turn; *mig-17*, *-18*, and *-19* affect it after the first turn; and *mig-20* affects it after the second turn. However, this idea is not consistent with the fact that *vab-3*, which affects DTC migration after the second turn, suppresses *mig-14*. One model to explain this complexity is to postulate an interaction between *vab-3* and *mig-14*. The expression of *vab-3* might be partly repressed in the posterior body region by wild-type *mig-14* activity, and it might be extended to the posterior body in a mutant *mig-14* background. In *mig-14* mutants, derepressed wild-type *vab-3* expression in the posterior region may cause a type II defect in the posterior DTC. Thus, in *vab-3; mig-14* double mutants, both DTCs could be similarly affected by the mutant VAB-3 protein and thus express the type I defect, exhibiting epistasis of *vab-3* to *mig-14*. In the case of the *vab-3(e648); mig-19* double mutant, *vab-3(e648)* suppressed *mig-19*, and concomitantly the slight *vab-3(e648)* posterior type II defect was strongly enhanced. *mig-19* may affect a process partly redundant with *vab-3* whose function is manifested when VAB-3 is depleted.

In *mig-14* and *mig-19* animals, migration of HSN neurons or Q neuroblasts (or their descendants) was also affected. HSN is born near the tail and migrates anteriorly. Q neuroblasts are born in the posterior body and migrate anteriorly (QR) or posteriorly (QL) while dividing in a stereotypical pattern (Sulston and Horvitz 1977). The effects of these mutations on such migratory cells in the anterior body region as ALM, CAN, and coelomocyte mother cells (mothers of ccLa/p and ccRa/p) were weak (Figure 7). These observations, together with the fact that *mig-14* and *mig-19* had stronger effects on posterior DTC migration, suggest that the *mig-14* and *mig-19* genes may be especially important for the migration of various cell types in the posterior body region.

mig-14; mig-20 and *mig-19; mig-20* double mutants showed abnormal movement. Because various genes have been reported that are required both for cell migration and axon outgrowth (Hedgecock *et al.* 1990; Wightman *et al.* 1996; Forrester and Garriga 1997), the strong uncoordinated movement phenotypes observed in these double mutants may be caused by defects in the migration of axons required to generate the neural connectivity essential for normal animal locomotion.

I thank Ed Hedgecock and members of his lab for introducing me to the fundamentals of *C. elegans* postembryonic development. I am grateful to Lee Honigberg, Edward Kipreos, John Plenefisch, Bruce Vogel, Yo Tabuse, and Tohru Sano for critical reading of the manuscript. I also thank Lee Honigberg and Cynthia Kenyon for *mig-14(mu71)*, Christina Borland and Michael Stern for *unc-71(ay7) bli-5(e518)*, and Theresa Stiernagle for various strains. I am grateful to Ed Hedgecock, Johji Miwa, Yo Tabuse, and Tohru Sano for discussions and encouragement and Saori Gouda and Toshie Miyamoto for technical assistance. Some *C. elegans* strains were provided by the *Caenorhabditis* Genetics Center, which is funded by the National Institutes of Health National Center for Research Resources.

LITERATURE CITED

Ambros, V., and H. R. Horvitz, 1984 Heterochronic mutants of the nematode *Caenorhabditis elegans*. Science **266:** 409–416.

Antebi, A., C. R. Norris, E. M. Hedgecock and G. Garriga, 1997 Cell and growth cone migrations, pp. 583–609 in *C. elegans* II, edited by D. L. Riddle, T. Blumental, B. Meyer and J. R. Priess. Cold Spring Harbor Laboratory Press, Cold Spring Harbor, NY.

Brenner, S., 1974 The genetics of *Caenorhabditis elegans*. Genetics **77:** 71–94.

Chan, S. S.-Y., H. Zheng, M.-W. Su, R. Wilk, M. T. Killeen *et al.*, 1996 UNC-40, a *C. elegans* homolog of DCC (Deleted in Colorectal Cancer), is required in motile cells responding to UNC-6 netrin cues. Cell **87:** 187–195.

Chen, E. B., C. S. Branda and M. J. Stern, 1997 Genetic enhancers of *sem-5* define components of the gonad-independent guidance mechanism controlling sex myoblast migration in *Caenorhabditis elegans* hermaphrodites. Dev. Biol. **182:** 88–100.

Chisholm, A. D., and H. R. Horvitz, 1995 Patterning of the *Caenorhabditis elegans* head region by the *Pax-6* family member *vab-3*. Nature **377:** 52–55.

Cowing, D. W., and C. Kenyon, 1992 Expression of the homeotic gene *mab-5* during *Caenorhabditis elegans* embryogenesis. Development **116:** 481–490.

Felix, M.-A., and P. W. Sternberg, 1996 Symmetry breakage in the development of one-armed gonads in nematodes. Development **122:** 2129–2142.

Forrester, W. C., and G. Garriga, 1997 Genes necessary for *C. elegans* cell and growth cone migrations. Development **124:** 1831–1843.

Harris, J., L. Honigberg, N. Robinson and C. Kenyon, 1996 Neuronal cell migration in *C. elegans*: regulation of Hox gene expression and cell position. Development **122:** 3117–3131.

Hedgecock, E. M., J. G. Culotti, D. H. Hall and B. D. Stern, 1987 Genetics of cell and axon migrations in *Caenorhabditis elegans*. Development **100:** 365–382.

Hedgecock, E. M., J. G. Culotti and D. H. Hall, 1990 The *unc-5*, *unc-6*, and *unc-40* genes guide circumferential migrations of

pioneer axons and mesodermal cells on the epidermis in *C. elegans.* Neuron **2:** 61–85.

Higgins, B. J., and D. Hirsh, 1977 Roller mutants of the nematode *Caenorhabditis elegans.* Mol. Gen. Genet. **150:** 63–72.

Hodgkin, J. A., 1980 More sex-determination mutants of *C. elegans*. Genetics **96:** 649–664.

Hodgkin, J. A., and S. Brenner, 1977 Mutations causing transformation of sexual phenotype in the nematode *Caenorhabditis elegans*. Genetics **86:** 275–287.

Horvitz, H. R., and J. E. Sulston, 1980 Isolation and genetic characterization of cell-lineage mutants of the nematode *Caenorhabditis elegans.* Genetics **96:** 435–454.

Ishii, N., W. G. Wadsworth, B. D. Stern, J. G. Culotti and E. M. Hedgecock, 1992 UNC-6, a laminin-related protein, guides cell and axon migrations in *C. elegans.* Neuron **9:** 873–881.

Keino-Masu, K., M. Masu, L. Hinck, E. D. Leonardo, S. S.-Y. Chan *et al.*, 1996 Deleted in Colorectal Cancer (DCC) encodes a netrin receptor. Cell **87:** 175–185.

Kenyon, C., 1986 A gene involved in the development of the posterior body region of *C. elegans.* Cell **46:** 477–487.

Kimble, J., and D. Hirsh, 1979 The postembryonic cell lineages of the hermaphrodite and male gonads in *Caenorhabditis elegans.* Dev. Biol. **87:** 396–417.

Leonardo, E. D., L. Hinck, M. Masu, K. Keino-Masu, S. L. Ackerman *et al.*, 1997 Vertebrate homologues of *C. elegans* UNC-5 are candidate netrin receptors. Nature **386:** 833–838.

Leung-Hagesteijn, C., A. M. Spence, B. D. Stern, Y. Zhou, M.-W. Su *et al.*, 1992 UNC-5, a transmembrane protein with immunoglobulin and thrombospondin type I domains, guides cell and axon migrations in *C. elegans.* Cell **71:** 289–299.

Lewis, J. A., and J. A. Hodgkin, 1977 Specific neuroanatomical changes in chemosensory mutants of the nematode *Caenorhabditis elegans.* J. Comp. Neurol. **172:** 489–510.

Manser, J., and W. B. Wood, 1990 Mutations affecting embryonic cell migrations in *Caenorhabditis elegans.* Dev. Genet. **11:** 49–64.

Salser, S. J., and C. Kenyon, 1996 A *C. elegans* Hox gene switches on, off, on and off again to regulate proliferation, differentiation and morphogenesis. Development **122:** 1651–1661.

Salser, S. J., C. M. Loer and C. Kenyon, 1993 Multiple HOM-C gene interactions specify cell fates in the nematode central nervous system. Genes Dev. **7:** 1714–1724.

Serafini, T., T. E. Kennedy, M. J. Galko, C. Mirzayan, T. M. Jessell *et al.*, 1994 The netrins define a family of axon outgrowth-promoting proteins homologous to *C. elegans* UNC-6. Cell **78:** 409–424.

Sigurdson, D. C., G. J. Spanier and R. K. Herman, 1984 *Caenorhabditis elegans* deficiency mapping. Genetics **108:** 331–345.

Stern, M. J., and H. R. Horvitz, 1991 A normally attractive cell interaction is repulsive in two *C. elegans* mesodermal cell migration mutants. Development **113:** 797–803.

Sternberg, P. W., and H. R. Horvitz, 1981 Gonadal cell lineages of the nematode *Panagrellus redivivus* and implications for evolution by the modification of cell lineage. Dev. Biol. **88:** 147–166.

Sulston, J. E., and H. R. Horvitz, 1977 Post-embryonic cell lineages of the nematode, *Caenorhabditis elegans.* Dev. Biol. **56:** 110–156.

Trent, C., N. Tsung and H. R. Horvitz, 1983 Egg-laying defective mutants of the nematode *Caenorhabditis elegans.* Genetics **104:** 619–647.

Tuck, S., and I. Greenwald, 1995 *lin-25*, a gene required for vulval induction in *Caenorhabditis elegans.* Genes Dev. **9:** 341–357.

Wadsworth, W. G., H. Bhatt and E. M. Hedgecock, 1996 Neuroglia and pioneer neurons express UNC-6 to provide global and local netrin cues for guiding migrations in *C. elegans.* Neuron **16:** 35–46.

Wightman, B., S. G. Clark, A. M. Taskar, W. C. Forrester, A. V. Maricq *et al.*, 1996 The *C. elegans* gene *vab-8* guides posteriorly directed axon outgrowth and cell migration. Development **122:** 671–682.

Williams, B. D., B. Schrank, C. Huynh, R. Shownkeen and R. H. Waterston, 1992 A genetic mapping system in *Caenorhabditis elegans* based on polymorphic sequence-tagged sites. Genetics **131:** 609–624.

Zhang, Y., and S. W. Emmons, 1995 Specification of sense-organ identity by a *Caenorhabditis elegans Pax-6* homologue. Nature **377:** 55–59.

Communicating editor: R. K. Herman